Applied Catalysis B: Environmental 306 (2022) 121128

Contents lists available at ScienceDirect

Applied Catalysis B: Environmental

journal homepage: www.elsevier.com/locate/apcatb

The effect of non-redox promoters (AlO_x, PO_x, SiO_x and ZrO_x) and surface sulfates on supported V_2O_5-WO_3/TiO_2 catalysts in selective catalytic reduction of NO with NH_3

Mingyu Guo [a,b,1], Bar Mosevitzky Lis [a,1], Michael E. Ford [a], Israel E. Wachs [a,*]

[a] Operando Molecular Spectroscopy & Catalysis Laboratory, Department of Chemical and Biomolecular Engineering, Lehigh University, Bethlehem, PA 18015, USA
[b] Tianjin Key Laboratory of Indoor Air Environmental Quality Control, School of Environmental Science and Engineering, Tianjin University, Tianjin 300350, China

ARTICLE INFO

Keywords:
SCR
Catalysts, supported V_2O_5-WO_3/TiO_2
Promoters, non-redox, alumina, phosphorous, silica, zirconia
Spectroscopy, Raman, Infrared
Temperature-Programmed Surface Reaction (TPSR)

ABSTRACT

The SCR activity of MO_x (M=Al, P, Si, Zr) promoted V_2O_5-WO_3/TiO_2 was investigated before and after sulfation. *In situ* IR spectroscopy indicated that the VO_x active sites preferentially anchor on promoter generated surface hydroxyl. *In situ* Raman spectroscopy confirmed that all oxides are completely dispersed on the TiO_2 surface. *In situ* NH_3-IR spectroscopy showed that the oxides can increase the Lewis (AlO_x and ZrO_x) and Brønsted (PO_x, SiO_x, VO_x, WO_x and SO_x) acid site concentrations. The SiO_x and ZrO_x promoters had little effect on NO conversion, while the AlO_x and PO_x promoters and surface sulfation generally inhibited it. The SiO_x promoted catalyst was highly SCR active despite lacking Lewis acid sites, indicating that they are not vital for SCR. The N_2O formation activity of the catalyst was inhibited by surface sulfation and the promoters, correlating with the promoter and SO_x induced increase in the Brønsted acid sites' strength.

1. Introduction

Selective catalytic reduction (SCR) of NO_x with NH_3 using the supported V_2O_5-WO_3/TiO_2 catalyst is widely applied to control NO_x emissions from power plants and industrial boilers [1–3]. While VO_x surface species act as the active sites, surface impregnated WO_x generates additional surface acid sites and promotes the redox activity. This promotional effect has been suggested to be either electronic [4,5], or more likely considering the identical NO conversion of 1%V_2O_5/TiO_2 and 1% V_2O_5-1%WO_3/TiO_2 catalysts [6], due to surface VO_x oligomerization [3,5,6]. The supported V_2O_5-WO_3/TiO_2 catalyst reaches its maximum NO_x conversion at ~300–400 °C [7,8], but generates the greenhouse gas N_2O at high temperatures by over oxidizing the NH_3, especially in dry conditions [9]. Achieving high SCR activity at low temperatures is thus desirable as it enables the utilization of SCR in mobile combustion applications even under "cold start" conditions [10] as well as minimizes N_2O emissions. Sulfur dioxide (SO_2), formed when sulfur present in fossil fuels is oxidized during the combustion process, can oxidize to sulfur trioxide (SO_3) [11]. Surface sulfates have been reported to either deactivate the V_2O_5-WO_3/TiO_2 catalyst by blocking and poisoning the active surface sites [12], or promote its SCR activity by strengthening the Lewis acid sites, increasing the number of Brønsted acid sites, and affecting the active sites *via* a ligand effect [13,14]. Oxidation of SO_2 on the catalyst surface is undesired as it forms surface sulfates that poison the catalysts [15] and lead to detrimental downstream sulfate deposition [15,16]. Furthermore, the release of SO_3 to the atmosphere contributes to the formation of smog and acid rain [17]. Unfortunately, the supported V_2O_5-WO_3/TiO_2 SCR catalyst is incapable of achieving high SCR activity at low temperatures and is highly active in SO_2 oxidation.

It is common practice in industrial-scale SCR to promote V_2O_5-WO_3/TiO_2 catalysts with Al_2O_3, P_2O_5, SiO_2 and ZrO_2 for SO_2 and water vapor containing flue gas treatment [18–22]. These promoters have been previously studied in the literature. Impregnation of Al_2O_3 onto a V_2O_5-WO_3/TiO_2 catalyst irreversibly decreases the acid site concentration, leading to catalyst deactivation [23,24], though the resulting catalyst improves in performance after sulfation possibly due to the neutralization of the more basic AlO_x sites by the deposited SO_x [24]. The impregnation of P_2O_5 on V_2O_5-WO_3/TiO_2 generates additional Lewis and Brønsted surface acid sites [25–27] which are either stronger [26] or of similar strength [27], increases the extent of surface VO_x oligomerization [25], and either increases [25,27,28] or decreases [26–29] the NO conversion. When SiO_2 is present in the support as

* Corresponding author.
E-mail address: iew0@lehigh.edu (I.E. Wachs).
[1] Mingyu Guo and Bar Mosevitzky Lis contributed equally to this work

https://doi.org/10.1016/j.apcatb.2022.121128
Received 15 October 2021; Received in revised form 17 January 2022; Accepted 19 January 2022
Available online 22 January 2022

V_2O_5/SiO_2-WO_3-TiO_2 it increases the number of surface acid sites [30–32], mildly decreases the acid strength [30] and either increases [31] or decreases [30,32] the NO conversion. When SiO_2 is impregnated on the surface either with (SiO_2-V_2O_5-WO_3/TiO_2) [33] or right before ($V_2O_5/SiO_2/WO_3$-TiO_2) [34] the V_2O_5, the NO conversion still decreases at low temperatures but increases at higher temperatures relative to the SiO_2 free catalyst. For V_2O_5-WO_3/SiO_2-TiO_2 supported catalysts, sulfates preferentially anchor on Si surface hydroxyls, while the presence of Si in the support affords superior SO_2 poisoning resistance to the catalyst [35]. When ZrO_2 is present either on the surface (V_2O_5-ZrO_2/TiO_2-WO_3) [36] or in the support (V_2O_5-WO_3/TiO_2-ZrO_2) [37] it enhances SCR performance and selectivity, and improves the catalyst's thermal stability despite decreasing or even eliminating the Brønsted acid sites. There are no previous studies in the literature that summarize and directly compare the effect of these non-redox promoters on the surface molecular structures and SCR activity of supported V_2O_5-WO_3/TiO_2 catalysts, thereby enabling the assessment of these promoters relative to one another.

In this work, AlO_x, PO_x, SiO_x and ZrO_x promoted, sulfated and sulfate-free, supported V_2O_5-WO_3/TiO_2 catalysts were synthesized by the incipient-wetness impregnation method. Metal oxide anchoring sites and molecular structures of the catalysts were characterized by *in situ* Raman and Infrared (IR) spectroscopies, and their surface acidity was probed with IR-NH_3 temperature programmed desorption. The NO conversion and N_2O selectivity of the catalysts as a function of the surface non-redox promoters (AlO_x, PO_x, SiO_x and ZrO_x) was investigated by Temperature-Programmed Surface Reaction (TPSR). Overall, the results reported herein enable linking the surface molecular structures to the catalytic performance of the non-redox promoted, sulfated and sulfate-free, supported V_2O_5-WO_3/TiO_2 catalysts, and evaluate these relations using a unified basis of comparison for the non-redox promoters.

2. Experimental section

2.1. Catalyst preparation

Incipient wetness impregnation was utilized to synthesize all the TiO_2 supported catalysts reported in this work. Sub-monolayer coverages are ideal for investigating catalytic structure–activity/selectivity relationships in supported catalysts, as they allow the formation of fully exposed monomeric and polymeric surface structures but not nanoparticles [38]. The 80% monolayer Al, P, Si and Zr surface coverages used here were achieved by using loadings that were calculated according to Equation S1 [39]. Previous work indicate that the monolayer weight loadings of Al_2O_3, P_2O_5, SiO_2 and ZrO_2 on TiO_2, respectively, are 2.6%, 5.0%, 6.2% and 4.0% [39–42]. Initially, 80% monolayer coverages of Al_2O_3 (2.1 wt%, precursor: $Al(NO_3)_3.9H_2O$, Alfa aesar), P_2O_5 (4.0 wt%, precursor: 86.8 wt% H_3PO_4 aqueous solution, Alfa aesar), SiO_2 (5.0 wt%, precursor: $Si(OC_2H_5)_4$, Sigma-Aldrich) and ZrO_2 (3.2 wt %, 70 wt% $Zr(OCH_2CH_2CH_3)_4$ in n-propoxide, Alfa aesar) were impregnated on TiO_2 (Evonik P-25; ~55 m^2/g; ~80% anatase and ~20% rutile). The SiO_2 and ZrO_2 promoted catalysts were synthesized in a glove box. The non-redox promoters' precursor solutions were added to the TiO_2 in a drop-wise manner under constant stirring. After 45 min of mixing, the samples were dried overnight at room temperature and then dehydrated under synthetic air (Airgas, 100 cc min^{-1}) at 120 °C for 2 hr and calcined at 450 °C (heating at a rate of 1 °C min^{-1}) for 4 hr. Subsequently, 1 wt% V_2O_5 (precursor: NH_4VO_3, Alfa Aesar) was impregnated onto the non-redox promoted TiO_2, which was then dried and calcined according to the same procedure detailed above. This was followed by the impregnation of 5 wt% WO_3 (precursor: $(NH_4)_6H_2W_{12}O_{40}{\cdot}XH_2O$, Strem Chemicals), dehydration and then calcination. Lastly, 1.5 wt% SO_4 (1.5 wt%, precursor: $(NH_4)_2SO_4$, Sigma-Aldrich) was impregnated onto the catalysts, which were dried and calcined a final time.

2.2. Catalyst characterization

2.2.1. BET specific surface area measurement

The surface areas of the catalysts were measured by N_2 adsorption-desorption (BET) using 100 mg samples with an ASAP 2020 HD88 (Micromeritics, USA). Prior to the measurement, the catalysts were dehydrated at 300 °C for 5 hr to remove moisture and any adsorbed impurities from their surface.

2.2.2. In situ Raman spectroscopy

In situ Raman measurements of the catalysts' molecular structures were performed with a 532 nm wavelength laser excitation on a single stage Horiba-Jobin Yvon Laboratory Ram-HR Raman spectrometer with a confocal microscope (Olympus BX-30) and a notch filter (Kaiser Super Notch). The beam was generated by a Nd-YAG double diode pumped laser (Coherent Compass 315 M-150, output power of 150 mW with power at the sample of 10 mW). The scattered photons were directed into a single monochromator and focused unto a UV-sensitive liquid N_2 cooled charge coupled device detector (Horiba-Jobin Yvon CCD-3000 V) with a spectral resolution of ~1 cm^{-1} at the applied parameters. Powder samples were loaded into a reaction cell (Harrick Scientific HVC-DRP4) and connected to a gas flow control system. The sample temperature was controlled by a Harrick ATC Temperature Controller unit. The catalysts were dehydrated by flowing 10% O_2/Ar (Airgas, 30 cc min^{-1}) at 400 °C for 1 hr prior to the Raman spectra acquisitions at 400 °C. The data used to plot the relevant Raman figures presented herein is provided in the SI.

2.2.3. In situ Infrared spectroscopy

In situ IR spectra were collected with a Fourier-transform infrared (FTIR) spectrometer (Thermo NICOLET 8700) equipped with a high sensitivity mercury-cadmium-telluride (MCT-A) detector and a Harrick Praying Mantis Attachment (Model DRA-2) for diffuse reflectance spectroscopy. Powder samples were loaded into a Harrick Scientific cell (HVC-DRP4) which was directly connected to a gas flow control system. The reaction chamber's temperature was controlled by a Harrick ATC Temperature Controller unit. In each experiment, the catalyst was heated to 400 °C (heating at a rate of 10 °C min^{-1}) and held for 1 hr under 10% O_2/Ar (30 cc min^{-1}), after which the *in situ* IR spectra was collected for the dehydrated catalyst. Ammonia temperature programmed desorption (TPD) was used to measure and quantify the catalysts' acidity. To achieve this, each catalyst was cooled from 400 °C to 110/200 °C, held at that temperature under 2000 ppm NH_3/He (PRAXAIR, 35 cc min^{-1}) for 30 min, followed by flowing He (PRAXAIR, 30 cc min^{-1}) for another 30 min to purge unabsorbed NH_3. Finally, the catalyst was heated to 500 °C (heating at a rate of 10 °C min^{-1}) under He (30 cc min^{-1}). The IR spectra were then acquired at 1 min intervals. All *in situ* IR spectra intensities were normalized using the TiO_2 support's IR band at ~920 cm^{-1}. The peaks at ~1230 cm^{-1} and ~1450 cm^{-1} were integrated to quantify the surface NH_3 * and NH_4^+* species on Lewis and Brønsted acid sites, respectively [7,43]. The data used to plot the relevant IR figures presented herein is provided in the SI.

2.2.4. Temperature-programmed surface reaction (TPSR) spectroscopy

The SCR activity of the catalysts was measured using an Altamira AMI-200 system equipped with a Dycor Dymaxion DME200MS online quadrupole mass spectrometer (MS). A U-type quartz tube loaded with 30 mg of catalyst fixed in place by quartz wool was used as a fixed-bed reactor. The catalysts were initially heated to 400 °C (heating at a rate of 10 °C min^{-1}) under 5% O_2/He (50 cc min^{-1}), soaking for 1 hr, and then cooled to 100 °C. After cooling, a 2000 ppm NH_3/He (35 cc min^{-1}), 2000 ppm NO/He (35 cc min^{-1}) and 5% O_2/He (5 cc min^{-1}) mixture was flowed into the reactor and the system was heated to 500 °C (heating at a rate of 10 °C min^{-1}). Outlet gas compositions were analyzed by the coupled MS to follow the catalytic activity as a function of temperature. The following mass to charge (m/z) ratios were used for species identification: NO ($m/z = 30$), N_2O ($m/z = 44$), NH_3 ($m/z = 17$),

N_2 (m/z = 28), H_2O (m/z = 18), and NO_2 (m/z = 46). No NO_2 was detected in any of the TPSR experiments described in this work. The data used to plot the relevant TPSR figures presented herein is provided in the SI.

3. Results and discussion

3.1. Anchoring surface sites of supported MO_x/TiO_2 catalysts

Impregnated metal oxides surface species are known to anchor at the surface hydroxyl sites that are present on metal oxide supports [44–46]. To examine the effects of the non-redox promoters on the anchoring of the VO_x, WO_x and SO_x surface sites, *in situ* IR spectra of the hydroxyl region (3450–3850 cm^{-1}) were acquired. The difference IR spectra comparing the hydroxyl region before and after promoter and 1%V_2O_5 impregnation on the TiO_2 support is presented in Fig. 1 with the original IR spectra provided in Figure S1. The TiO_2 support exhibited both more acidic bridging Ti-(OH)-Ti (3630, 3660 and 3674 cm^{-1}) and more basic terminal Ti-(OH) (3710 cm^{-1}) surface hydroxyls [43,47,48]. The impregnated VO_x surface sites titrated most of the Ti-(OH) and some of the Ti-(OH)-Ti (3674 cm^{-1}) surface hydroxyls while forming new V-(OH)-Ti surface hydroxyls at 3640 cm^{-1} [49,50]. The impregnation of 2.1%Al_2O_3 onto the TiO_2 support resulted in the consumption of a small portion of the more acidic Ti-(OH)-Ti surface hydroxyls at 3660 and 3630 cm^{-1} and the formation of more basic Al-(OH) (3768 cm^{-1}) and Al-(OH)-Al (3710 cm^{-1}) surface hydroxyls (Fig. 1a) [51–54]. Further impregnation of 1%V_2O_5 titrated the more basic Al-(OH) (3768 cm^{-1}), Al-(OH)-Al and Ti-(OH) (both vibrating at 3710 cm^{-1}) surface hydroxyls on 2.1%Al_2O_3/TiO_2 (Fig. 1a). The impregnation of PO_x completely titrated the basic Ti-(OH) (3710 cm^{-1}) surface hydroxyls and produced more acidic terminal P-(OH) (3660 cm^{-1}) [55] and possibly other unidentified (3541 cm^{-1}) surface hydroxyls (Fig. 1b). Impregnation of 1% V_2O_5 onto the PO_x promoted support only titrated a small amount of P-(OH) and Ti-(OH)-Ti (both vibrating at 3660 cm^{-1}) surface hydroxyls (Fig. 1b). The anchoring of SiO_x generated terminal Si-(OH) (3660 cm^{-1} and 3773 cm^{-1}) [56,57] (Fig. 1c). Both the Si-(OH) and Ti-(OH)-Ti (3630, 3660 and 3773 cm^{-1}) surface hydroxyls were consumed by the anchoring of VO_x species on the SiO_x promoted support (Fig. 1c). Lastly, the addition of ZrO_x produced both terminal Zr-(OH) (3750 cm^{-1}) and bridging Zr-(OH)-Zr (3710 cm^{-1} and 3664 cm^{-1}) [58–60] surface hydroxyls (Fig. 1d). The impregnation of 1%V_2O_5 onto 3.2%ZrO_2/TiO_2 titrated a large amount of surface hydroxyl species including Zr-(OH) (3750 cm^{-1}), Ti-(OH) (3710 cm^{-1}), Zr-(OH)-Zr (3664 and 3710 cm^{-1}) and Ti-(OH)-Ti (3660 and 3630 cm^{-1}) (Fig. 1d). The promotion of the TiO_2 support with these promoters generated new hydroxyls decreasing in acidity in the following order: 4.0%P_2O_5 > 3.2%ZrO_2 > 2.1%Al_2O_3 > 5.0%SiO_2 [47]. While the AlO_x and PO_x surface sites anchored on more acidic and basic Ti-hydroxyls, respectively, no hydroxyl consumption was detected for SiO_x and ZrO_x impregnation, suggesting that the produced and consumed hydroxyls shared similar wavelengths in those cases. These newly formed promoter surface hydroxyls were preferentially anchored upon by the VO_x sites, suggesting a possible ligand effect on the V active sites.

Impregnation of 5% WO_3 onto the unpromoted supported 1%V_2O_5/TiO_2 catalyst titrated additional Ti-(OH)-Ti (3660 cm^{-1}) surface hydroxyls as shown in Fig. 2 with the original IR spectra provided in Figure S2. The WO_x surface sites completely consumed the most basic Al-(OH) (3768 cm^{-1}), and partially titrated the less basic Ti-(OH), Al-(OH)-Al (3710 cm^{-1}) and Ti-(OH)-Ti (3660 cm^{-1}) surface hydroxyls on the AlO_x promoted catalyst (Fig. 2a). Conversely, 5%WO_3 impregnation onto the PO_x promoted catalysts titrated the moderately acidic P-(OH) and Ti-(OH)-Ti (both vibrating at 3660 cm^{-1}) surface hydroxyls (Fig. 2a). The anchoring of the surface WO_x species on the 1%V_2O_5/5.0%SiO_2/TiO_2 catalyst titrated some of the basic Si-(OH) (3733 cm^{-1}) and possibly some of the more acidic Si-(OH) and Ti-(OH)-Ti (3660 cm^{-1}) surface hydroxyls (Fig. 2b). For the ZrO_x promoted

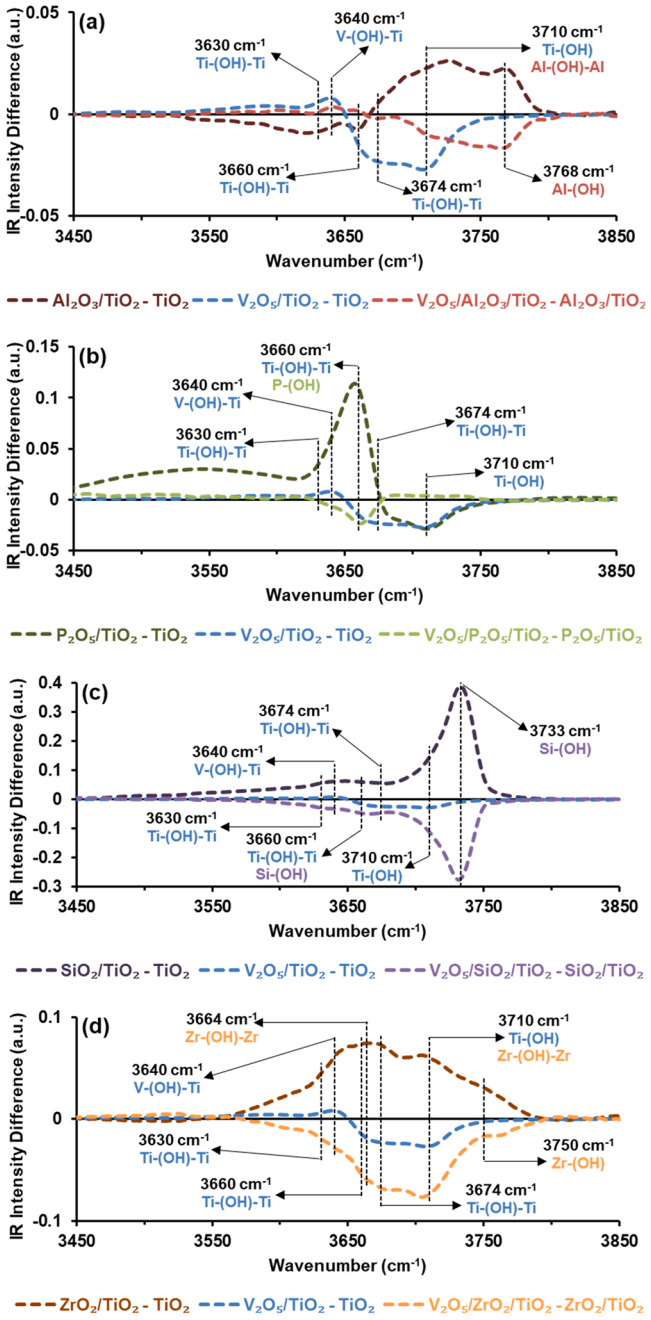

Fig. 1. *In situ* IR difference spectra of the hydroxyl region of dehydrated TiO_2 supported VO_x-free and VO_x impregnated (a) AlO_x promoted, (b) PO_x promoted, (c) SiO_x promoted and (d) ZrO_x promoted catalysts (spectra collected at 400 °C under 10% O_2/Ar flow). Non-uniform Y-axis were used to improve readability.

catalyst, mostly moderately acidic Ti-(OH)-Ti (3660 cm^{-1}) and Zr-(OH)-Zr (3664 cm^{-1}), as well as some Ti-(OH)-Ti (3674 cm^{-1}) and Zr-(OH) (3750 cm^{-1}) surface hydroxyls were anchored on by the WO_x (Fig. 2b). These results suggest that similarly to impregnated 1%V_2O_5, the WO_x surface sites preferentially anchor on the promoter surface hydroxyls.

The *in situ* IR difference spectra of the surface hydroxyl region for the dehydrated sulfated catalysts are presented in Fig. 3 with the original IR spectra provided in Figure S3. Sulfation of the unpromoted catalyst consumed some of the remaining Ti surface hydroxyls (Fig. 3). Surface sulfates anchored on the more basic Al-(OH)-Al, Ti-(OH) (3710 cm^{-1}) and Ti-(OH)-Ti (3674 cm^{-1}) surface hydroxyls on the AlO_x promoted catalyst, and on the moderately acidic Ti-(OH)-Ti and P-(OH)

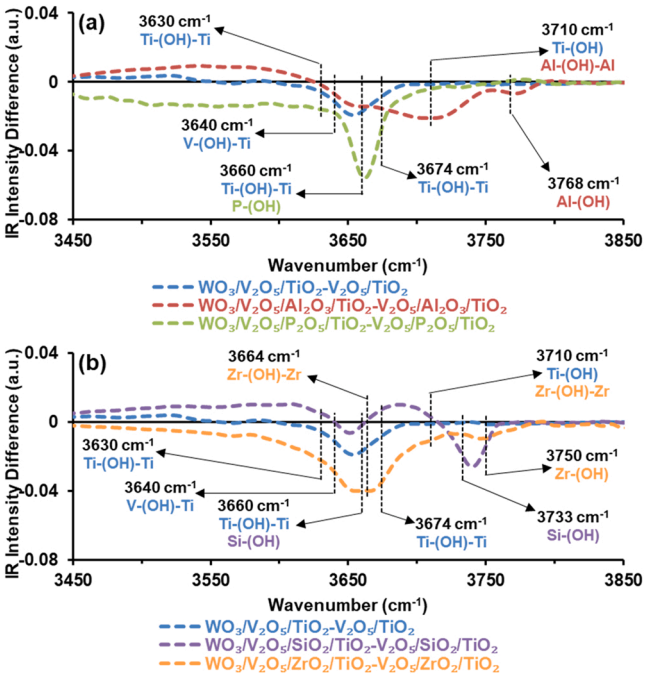

Fig. 2. *In situ* IR difference spectra of the hydroxyl region of the WO_x impregnated dehydrated (a) AlO_x promoted, PO_x promoted, (c) SiO_x promoted and ZrO_x promoted $1\%V_2O_5/TiO_2$ catalysts (spectra collected at 400 °C under 10% O_2/Ar flow).

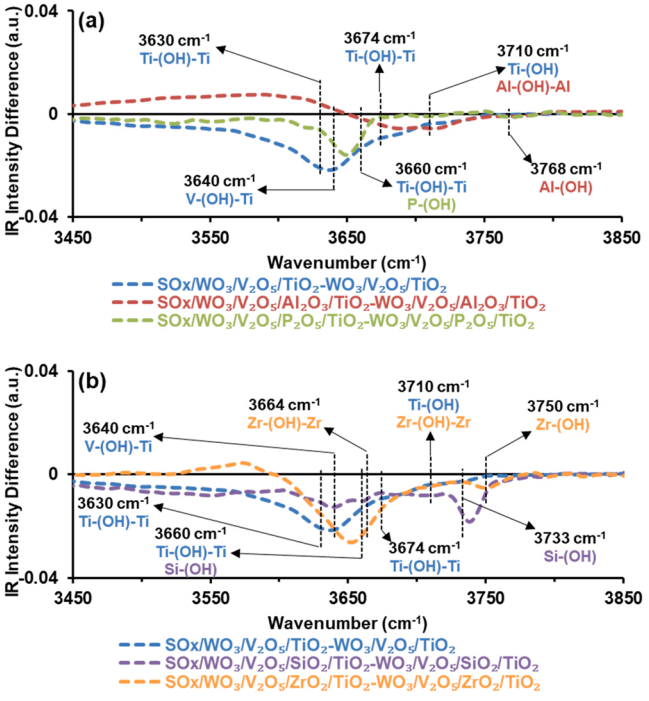

Fig. 3. *In situ* IR difference spectra of the hydroxyl region of the sulfated dehydrated (a) AlO_x promoted, PO_x promoted, (c) SiO_x promoted and ZrO_x promoted $1\%V_2O_5$-$5\%WO_3/TiO_2$ catalysts (spectra collected at 400 °C under 10% O_2/Ar flow).

($3660\ cm^{-1}$) surface hydroxyls of the PO_x promoted catalyst (Fig. 3a). Surface SO_x sites titrated small fractions of the various Si and Ti surface hydroxyls present on the $5\%WO_3/1\%V_2O_5/5.0\%SiO_2/TiO_2$ catalyst (Fig. 3b). While mostly acidic Ti-(OH)-Ti (3630 and $3660\ cm^{-1}$), V-(OH)-Ti ($3640\ cm^{-1}$) and Zr-(OH)-Zr ($3664\ cm^{-1}$) surface hydroxyls were anchored on during the impregnation of SO_x on the ZrO_x promoted catalyst, some of the more basic Ti-(OH)-Ti ($3674\ cm^{-1}$), Ti-(OH), Zr-(OH)-Zr ($3710\ cm^{-1}$) and Zr-(OH) ($3750\ cm^{-1}$) surface hydroxyls were consumed as well (Fig. 3b). Although promoter surface hydroxyls were also titrated during sulfation, significant amounts of Ti surface hydroxyls were consumed as well, partially due to the depletion of the promoter hydroxyls as was the case for the Al-(OH) ($3768\ cm^{-1}$) surface hydroxyls (Fig. S3a). Overall, the variable surface hydroxyl distributions and acidities discussed above suggest that the anchoring of impregnated VO_x, WO_x and SO_x is highly affected by the presence of the promoters, possibly influencing the catalytic performance by ligand effects.

3.2. *Molecular structure of surface MO_x sites on TiO_2*

As shown in Fig. 4, the *in situ* Raman spectrum of the TiO_2 support was dominated by its anatase vibrations (~384, 512, 623 cm^{-1} [61,62] and its weak second-order feature at ~799 cm^{-1} [63]), overwhelming the rutile (~20% wt) vibrations due to poorer scattering by the latter phase. The Raman spectra of the promoted TiO_2 lacked the strong Raman bands rising from Al_2O_3 (δ- 251 cm^{-1}, α- 416 cm^{-1}) [64], P_2O_5 (685 cm^{-1}) [65] SiO_2 (970 cm^{-1}) [66] and ZrO_2 (330 and 469 cm^{-1}) [67,68] nanoparticles, suggesting they were fully dispersed on the TiO_2 support (Fig. 4). The lack of V_2O_5 (997 cm^{-1}) and WO_3 (805 cm^{-1}) nanoparticle Raman bands in the unpromoted supported $5\%WO_3/1\%V_2O_5/TiO_2$ catalyst combined with the presence of surface VO_x (~1031 cm^{-1}) and WO_x (~1013 cm^{-1}) bands (Fig. 4) confirmed the complete dispersion of the VO_x and WO_x surface species [47]. The lack of bands typical of $AlVO_4$ (991 cm^{-1}) [69], $Al_2(WO_4)_3$ (1052 cm^{-1}) [70], $VOPO_4$ (923 cm^{-1}) [71], ZrV_2O_7 (769 cm^{-1}) [72], $Zr(WO_4)_2$ (750 cm^{-1}) [70] on the promoted supported $5\%WO_3/1\%V_2O_5/TiO_2$ catalyst indicated the redox species do not form distinct particles with the promoters on the surface.

The overtone region of the V=O and W=O bands, accessible by *in situ* IR spectroscopy, is twice as sensitive to vibrational shifts as any relative shift is approximately doubled in value thereby making it more discernable, and was therefore used to study the dynamic

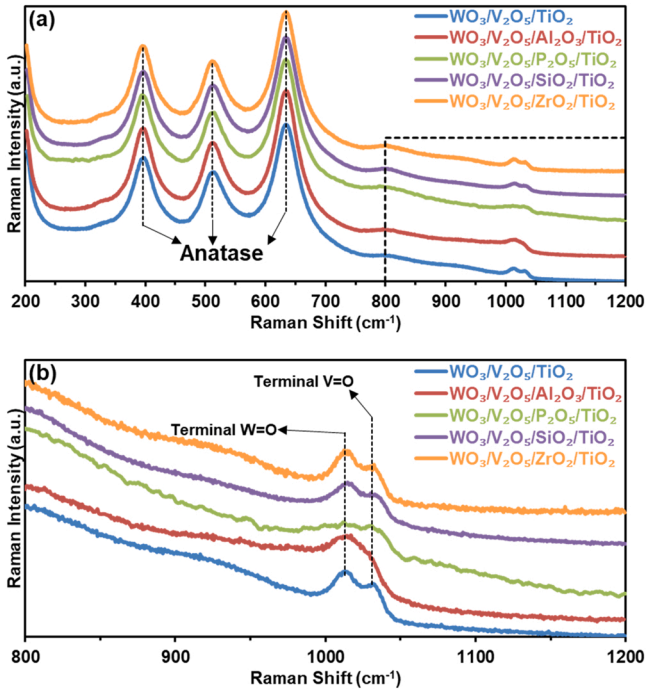

Fig. 4. *In situ* Raman spectra of dehydrated non-redox promoted supported 5% $WO_3/1\%V_2O_5/TiO_2$ catalysts at 400 °C in flowing 10% O_2/Ar for the spectral regions of (a) 200–1200 cm^{-1} and (b) 800–1200 cm^{-1}.

oligomerization of the redox sites (Fig. 5). The V═O vibration on the unpromoted support (2039 cm^{-1}) red shifted to lower wavenumbers (2028–2037 cm^{-1}) when the 1%V_2O_5 was impregnated on the promoted TiO_2, with the exception of the PO_x promoted support where the V═O vibration blue shifted to 2041 cm^{-1}. This demonstrates that the non-redox promoters affect the VO_x surface molecular structure by decreasing (AlO_x, SiO_x and ZrO_x) or increasing (PO_x) the extent of VO_x oligomerization. Previous work in which 1%P_2O_5 and 1%V_2O_5 were co-impregnated onto a 5%WO_3/TiO_2 surface similarly resulted in increased VO_x oligomerization as confirmed by ^{51}V NMR and *in situ* Raman [25].

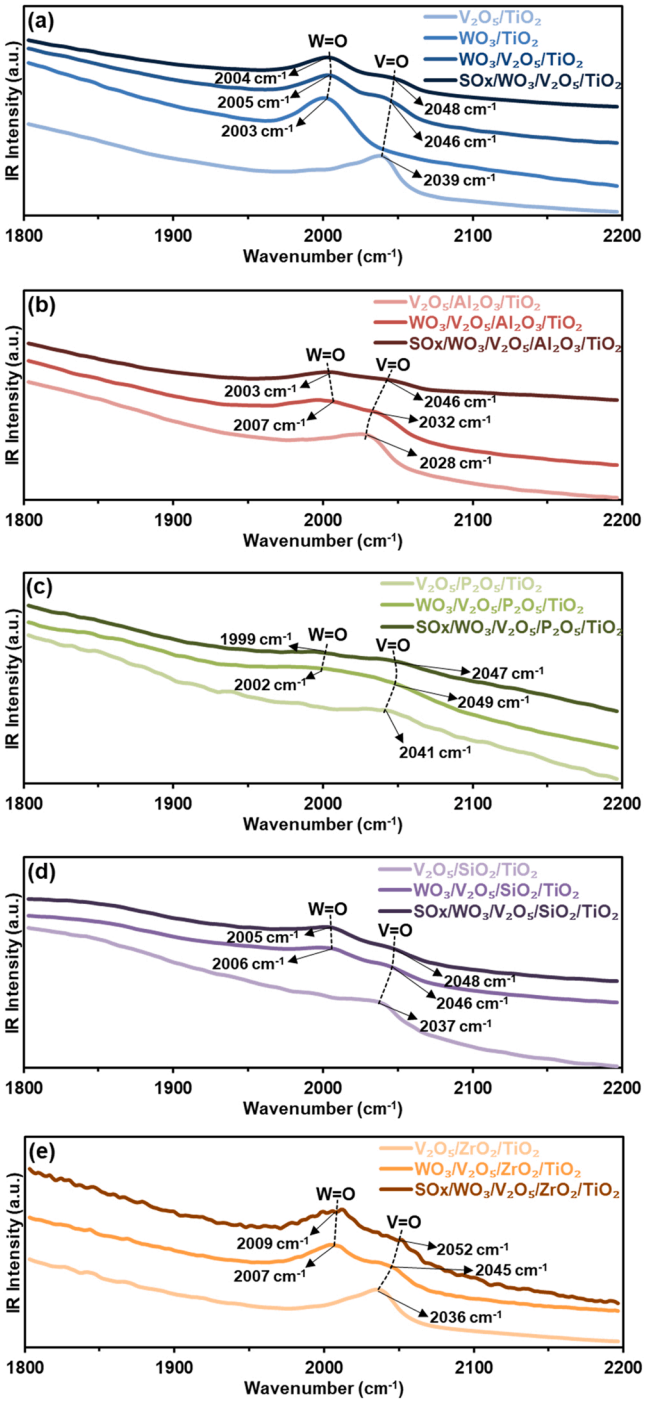

Fig. 5. *In situ* IR spectra of the overtone region for the dehydrated (a) unpromoted catalysts, (b) AlO_x promoted catalysts, (c) PO_x promoted catalysts, (d) SiO_x promoted catalysts, and (e) ZrO_x promoted catalysts (spectra collected at 400 °C in flowing 10% O_2/Ar).

The impregnation of 5%WO_3 introduced a new W═O vibration at 2005 cm^{-1} and blue shifted the V═O band to 2046 cm^{-1}, reflecting the oligomerizing effect of WO_x on the VO_x surface structures [6]. This increase in VO_x oligomerization was detected on the WO_x impregnated promoted catalysts as well, with the V═O vibration blue shifting to 2032–2049 cm^{-1}. The W═O vibration was blue shifted to ~2007 cm^{-1} by the AlO_x, SiO_x and ZrO_x promoters and red shifted to 2002 by the PO_x promoter, reflecting increasing and decreasing WO_x surface site oligomerization, respectively. Sulfation further blue shifted the V═O vibration to 2048 cm^{-1} in the unpromoted catalyst, and to 2046–2052 cm^{-1} in the AlO_x, SiO_x and ZrO_x promoted catalysts, suggesting further VO_x oligomerization. Only on the PO_x promoted catalyst did the V═O band red shift to 2047 cm^{-1} due to sulfation, reflecting a decrease in the VO_x oligomerization. The W═O vibration in the unpromoted and SiO_x promoted catalysts was only negligibly affected by sulfation and was either red shifted (AlO_x and PO_x) or blue shifted (ZrO_x) on the other promoted catalysts. The changes in the V═O and W═O IR overtone vibrations due to the non-redox promoters and sulfates as discussed above demonstrate that oligomeric species do exist on the surface despite the inability to confirm their presence *via* Raman spectroscopy due to the interference of the strong Anatase phase band at 796 cm^{-1} with the V-O-V (750–830 cm^{-1}) and W-O-W (~780 cm^{-1}) Raman bands. Compared to the unpromoted catalyst, only the AlO_x promoted catalyst exhibited significantly lower VO_x oligomerization after 5%WO_3 impregnation, with the V═O band vibrating 14 cm^{-1} wavenumbers lower (2046 *vs* 2032 cm^{-1}). Once sulfated, V═O band on the AlO_x promoted catalyst blue shifted to approximately the same wavenumber as on the sulfated unpromoted catalyst, but the band on the ZrO_x promoted catalyst blue shifted to 2052 cm^{-1}, reflecting higher VO_x oligomerization than both the unpromoted and other non-redox promoted sulfated catalysts. These results demonstrate the dynamic relation between the molecular structure of the VO_x surface sites and the non-redox promoters and sulfate on the catalyst surface.

The *in situ* IR spectra for the sulfate region of the dehydrated sulfated catalysts are plotted in Fig. 6. The S═O vibration at 1360–1380 cm^{-1} was indicative of the asymmetric stretch of mono-oxo O═S(-O)$_3$ surface sulfate sites [11]. The blue shift of the S═O band on the non-redox promoted catalysts relative to its unpromoted counterpart suggests that the interactions with the promoters affected the structural distortion of the SO_4 surface site. A weak IR band at ~1300 cm^{-1} was present in some of the spectra, indicating the presence of a secondary sulfate species since S-O-M bands only vibrate at lower wavenumbers (< 1200 cm^{-1}) [60,73].

3.3. Surface acidity of supported MO_x/TiO_2 catalysts

3.3.1. Effect of promoters and surface sulfates

The NH_3 * and NH_4^+* surface species concentrations on Lewis and Brønsted acid sites, respectively, were monitored with *in situ* IR spectroscopy after ammonia was adsorbed on the catalysts' surfaces. The concentrations of the Lewis and Brønsted surface acid sites on the

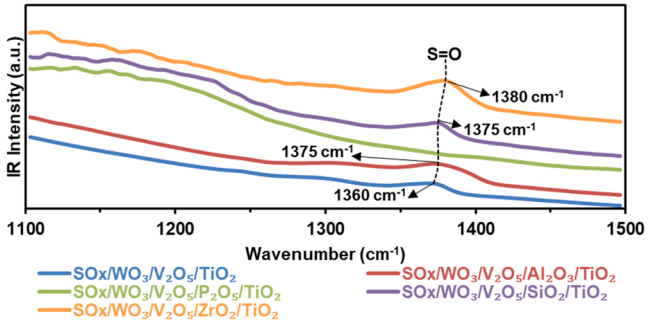

Fig. 6. *In situ* IR spectra of the dehydrated sulfated catalysts.

sulfated and sulfate-free promoted and unpromoted supported 5%WO_3/1%V_2O_5/TiO_2 catalysts are provided in Table S1 and plotted in Fig. 7. The effect of the impregnated AlO_x, PO_x, SiO_x and ZrO_x surface species on the surface acidity of the TiO_2 support is presented in Fig. 7a. As measured in previous literature, only Lewis acid sites were detected on the TiO_2 support [47,74], with promotion by 2.1%Al_2O_3 and 3.2%ZrO_2 slightly decreasing and increasing the Lewis acid site concentration, respectively, while generating no Brønsted acid sites. Conversely, impregnation of 4%P_2O_5 and 5%SiO_2 eliminated the TiO_2 Lewis acid sites and generated new Brønsted acid sites, with ~5 times more Brønsted acid sites on the PO_x promoted catalyst compared to the SiO_x promoted catalyst. Although the impregnations of VO_x and WO_x onto TiO_2 (Fig. 7b and 7c) decreased the Lewis acid site concentration, they generated surface Brønsted acid sites, reflecting their Brønsted acid character. Impregnation of VO_x and WO_x (Fig. 7b and 7c) on supported 2.1%Al_2O_3/TiO_2 and 5%SiO_2/TiO_2 and 3.2%ZrO_2/TiO_2 progressively increased the concentration of Brønsted acid sites on these catalysts. When VO_x was added to the PO_x promoted catalyst, no change in the concentration of Brønsted acid sites was detected (Fig. 7b), although the Brønsted acid site concentration increased dramatically once WO_x was impregnated onto the catalyst (Fig. 7c). While the addition of VO_x decreased the concentration of Lewis acid sites in the AlO_x and ZrO_x promoted catalysts, the addition of WO_x increased it (Fig. 7b and 7c), contrasting the effect of WO_x impregnation on the other catalysts. Impregnation of Al_2O_3 onto a commercial V_2O_5-WO_3/TiO_2 was shown to decrease the Brønsted acid site concentration, in agreement with the results described above [23]. Zirconia present either on the surface (V_2O_5-ZrO_2/WO_3-TiO_2) or as part of the bulk (V_2O_5-WO_3/ZrO_2-TiO_2) has been shown to increase the concentration of Lewis acid sites [36] and decrease the Brønsted acid concentration [36,37]. This difference from the results reported above is explained by the fact that here the 3.2%ZrO_2 was impregnated onto TiO_2 which possessed only Lewis acid sites to anchor upon. No Lewis acid sites were formed due to VO_x and WO_x (Fig. 7b and 7c) impregnation on the PO_x and SiO- promoted catalysts, which displayed only Brønsted acid sites. While both SiO_2 and P_2O_5 was previously shown to generate both additional Brønsted and Lewis acid sites when co-impregnated with 1%V_2O_5 onto 3%WO_3/TiO_2, in this work they were directly impregnated onto the TiO_2 support, thereby completely titrating the TiO_2 Lewis acid sites [25–27,30–32]. Addition of surface SO_x generally increased the concentration of Brønsted acid sites in both the promoted and unpromoted catalysts (Fig. 7d). A major exception is the PO_x promoted catalyst which exhibited a decrease in the Brønsted acid site concentration due to the high acid site density induced by PO_x promotion. This unique behavior is probably due to the highly acidic nature of P_2O_5 [75], which was inhibited by the lower acid site density of the SO_x surface species. The Brønsted acid character of the SO_x surface species resulted in a decrease in Lewis acid sites, when such existed, in all catalysts with the exception of the AlO_x promoted catalyst (Fig. 7d). These results indicate that the acid character of the V_2O_5-WO_3/TiO_2 catalyst can be modified by promoting the TiO_2 support with non-redox promoters, with the Brønsted character inevitably strengthened with SO_x deposition on the surface unless strong acids (PO_x) are present on the surface to begin with.

3.3.2. *Strength of surface acid sites*

The acid sites' strengths were determined by the desorption temperatures of IR-monitored adsorbed NH_4^+* (Brønsted) and NH_3 * (Lewis) species on the catalysts (acid strength increases with desorption temperature) which are provided in Table 1. The Brønsted acid site strength was enhanced by the promoters in the sulfate-free 5%WO_3/1%V_2O_5/TiO_2 catalyst, with the Brønsted acid strength of each promoted catalyst increasing in the following order: PO_x > AlO_x > SiO_x > ZrO_x > unpromoted. A similar enhancement in Brønsted acid strength was previously observed for P_2O_5 impregnated catalysts [26]. Catalyst sulfation increased the Brønsted acid strength of the catalysts further, with the exception of the PO_x promoted catalyst's strength which decreased.

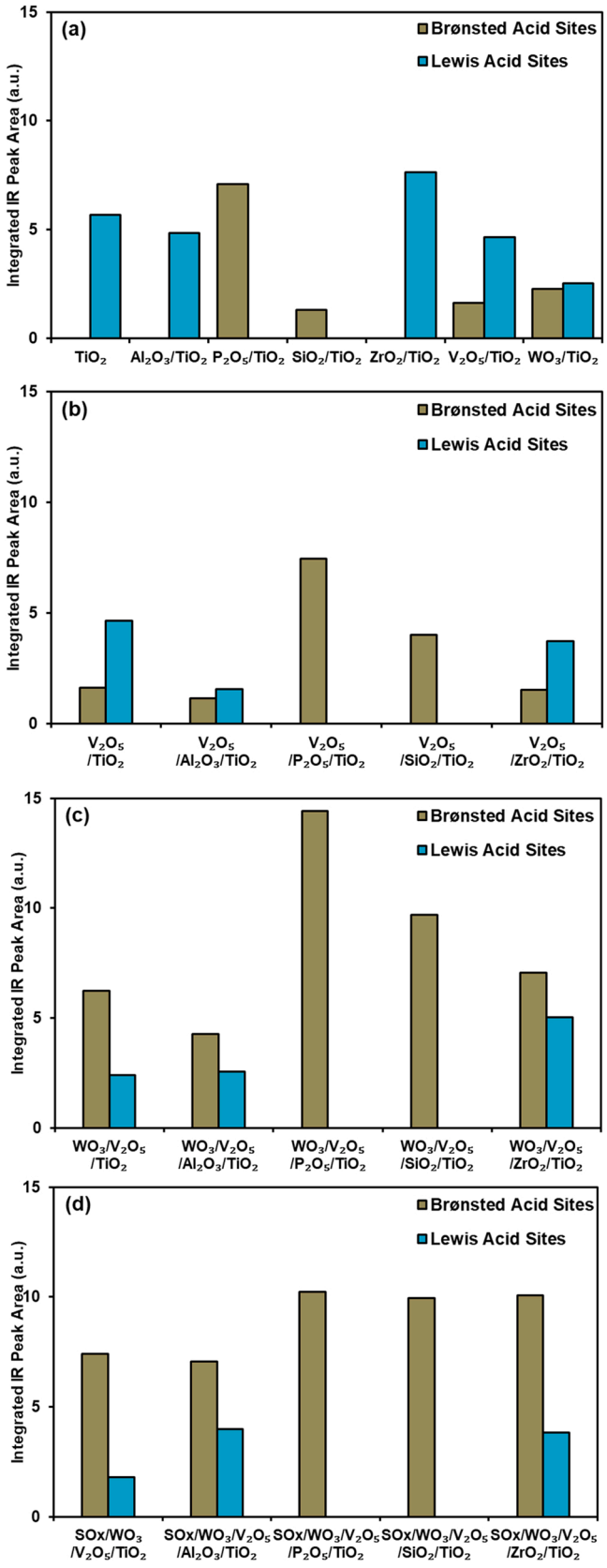

Fig. 7. Effect of surface MO_x on TiO_2 on the amount of surface Lewis and Brønsted acid sites as probed with ammonia adsorption-IR measurements at 110 °C in: (a) supported MO_x/TiO_2 catalysts, (b) supported VO_x impregnated catalysts, (c) supported WO_x impregnated catalysts and (d) supported SO_x impregnated catalysts.

Table 1
Desorption temperature of adsorbed ammonia species determined with *in situ* IR.

Samples	Desorption temperature of NH_4^+* from Brønsted acid sites (°C)	Desorption temperature of NH_3 * from Lewis acid sites (°C)
$WO_3/V_2O_5/TiO_2$	424	485
$WO_3/V_2O_5/Al_2O_3/TiO_2$	457	477
$WO_3/V_2O_5/P_2O_5/TiO_2$	487	–
$WO_3/V_2O_5/SiO_2/TiO_2$	456	–
$WO_3/V_2O_5/ZrO_2/TiO_2$	437	498
$SO_x/WO_3/V_2O_5/TiO_2$	463	480
$SO_x/WO_3/V_2O_5/Al_2O_3/TiO_2$	488	385
$SO_x/WO_3/V_2O_5/P_2O_5/TiO_2$	477	–
$SO_x/WO_3/V_2O_5/SiO_2/TiO_2$	476	–
$SO_x/WO_3/V_2O_5/ZrO_2/TiO_2$	467	457

Accordingly, the Brønsted acid strength order was similar after sulfation, with the exception of the PO_x promoted catalyst's strength now being lower than that of the AlO_x promoted catalyst. This reflects the strong Brønsted acid character of surface PO_x species[75], whose acid strength is higher than even the acidic surface SO_x species. The effect of the promoters on the Lewis acid strength of the catalyst varied, with ZrO_x and AlO_x promotion increasing and decreasing it, respectively. The increase in Lewis acid strength in the ZrO_x promoted catalyst agrees with previous literature where ZrO_2 was co-impregnated with V_2O_5 on a WO_3-TiO_2 mixed oxide [36]. While sulfation decreased the Lewis acid strength of all catalysts, the promoted catalysts were more affected, with their Lewis acid desorption temperature decreasing by ~40 °C (ZrO_x promoted) and ~90 °C (AlO_x promoted). With the exception of the sulfated promoted catalysts, the surface NH_3 * species desorbed from the Lewis acid sites at higher temperatures than from surface NH_4^+* species desorbed from the Brønsted acid sites, demonstrating the stronger acid strength of the Lewis acid sites. This was further reflected by the decrease in the Brønsted/Lewis acid site concentration ratio with temperature for the unpromoted AlO_x and ZrO_x promoted catalysts (zero for the PO_x and SiO_x promoted catalysts due to lack of Brønsted acid sites) which is provided in Table S2 and presented in Figure S5. This behavior reflects the generally easier desorption of surface NH_4^+* species from Brønsted acid sites than surface NH_3 * species from Lewis acid sites. Overall, these results demonstrate the ability of AlO_x, PO_x, SO_x and ZrO_x surface sites to tune the acid site character and strength of the V_2O_5-WO_3/TiO_2 SCR catalyst.

3.4. SCR-TPSR of unpromoted and non-redox promoted supported MO_x/TiO_2 catalysts

The supported MO_x/TiO_2 catalysts were chemically probed by NO/NH_3/O_2-TPSR and their NO conversion and N_2O formation activities are presented in Fig. 8, while the coupled N_2 selectivity is provided in Figure S6. The unpromoted supported 5%WO_3/1%V_2O_5/TiO_2 catalyst became SCR active at ~180 °C and reached its maximal NO conversion activity (~90%) at ~370 °C, with conversion slightly decreasing above 400 °C due to over-oxidation of NH_3 [8] (Fig. 8a). The AlO_x and PO_x surface species inhibited the SCR activity of the catalyst as demonstrated by the lower maximum NO conversion values achieved by these

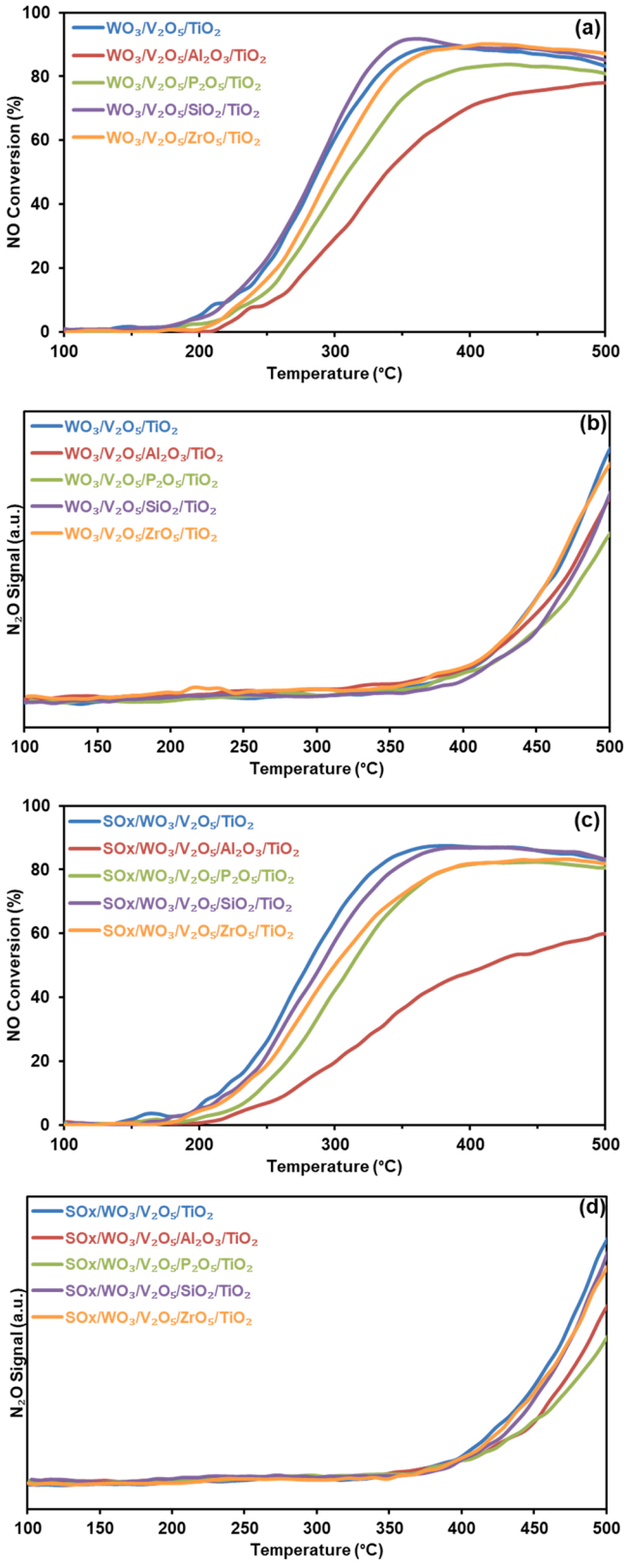

Fig. 8. Comparison of NO/NH_3/O_2-TPSR of unpromoted and non-redox promoted catalysts: (a) NO conversion over the sulfate-free catalysts, (b) N_2O formation over the sulfate-free catalysts, (c) NO conversion over the sulfated catalysts (d) and N_2O formation over the sulfated catalysts.

catalysts (78% and 84%, respectively). The inhibitory effect of AlO_x was previously demonstrated for an Al_2O_3-impregnated commercial V_2O_5-WO_3/TiO_2 catalyst [23], and similar loadings of P_2O_5 were shown to inhibit NO conversion for this catalyst system [26–29]. The SiO_x promoted catalyst exhibited similar performance to the unpromoted catalyst with the exception of the 295–390 °C temperature range, in which it reached a slightly higher maximum NO conversion value of ~92%. This similar performance was previously demonstrated in SiO_2 containing catalysts [31,33–35]. While the ZrO_x promoted catalyst was less SCR active at lower temperatures, it reached a similar maximum NO conversion value (~90%) above 390 °C when compared to the unpromoted catalyst. Improved high temperature NO conversion was reported before for a ZrO_2 and V_2O_5 co-impregnated WO_3-TiO_2 supported catalyst [36]. The N_2O formation activity of the unpromoted and promoted catalysts indicated that the AlO_x, PO_x and SiO_x promoted catalysts are less active in the formation of N_2O, while the ZrO_x promoted catalyst showed similarly high N_2O generation propensity at high temperatures (Fig. 8b). The SCR activity of the promoted catalyst was strongly affected by the catalyst sulfation, as shown in Fig. 8c. While the NO conversion activities of the unpromoted and PO_x promoted catalysts were not affected by the sulfation (Fig. S7a and S7e), the conversion for the SiO_x, ZrO_x and especially the AlO_x promoted catalysts was significantly inhibited (Fig. S7c, S7g and S7h), contradicting literature trends in the case of the latter [24]. The N_2O formation activity of the catalysts decreased after sulfation for the most part (Fig. 8d), with the unpromoted catalyst generating the same levels of N_2O (Fig. S7b) and the promoted catalysts all producing less N_2O (Fig. S7d, S7f, S7h and S7j). These results suggest that while promotion with SiO_2 is beneficial to the NO conversion activity of the V_2O_5-WO_3/TiO_2 SCR catalyst system and inhibits the formation of harmful N_2O, it does not maintain these positive effects when SO_x surface sites anchor to the catalyst's surface. Although some of the promoters do not enhance the NO conversion activity, the AlO_x and PO_x promoted catalysts maintain lower N_2O formation activity even after sulfation, while the PO_x promoted catalyst can maintain the same NO conversion activity it had before the sulfation. This behavior is probably due to the more acidic nature of the PO_x surface sites compared to the impregnated SO_x[75].

3.5. Surface structure-activity/selectivity relationships

The effect of the promoters on the SCR activity of the V_2O_5-WO_3/TiO_2 supported catalyst cannot be fully explained by the extent of VO_x oligomerization [6] since the highly oligomeric PO_x-promoted catalyst displayed the second-worst NO_x conversion activity. The seeming contradiction with previous literature suggests that while the extent of VO_x oligomerization can increase the low temperature NO conversion activity, other factors related to the presence of the non-redox promoters on the surface can negate this. The effect cannot be explained by the possible SCR activity of exposed promoter surface sites either, as all promoter impregnated TiO_2 support samples exhibited lower NO conversion activity than the bare TiO_2 support (Fig. S8), yet the SiO_x and ZrO_x promoted catalysts were slightly more SCR active at certain temperatures. Neither can the BET measured surface area (Table S2) of the catalysts explain the variation in SCR performance, nor can the concentration of Lewis or Brønsted acid sites (Fig. 7). In fact, this work demonstrates that a lack of Lewis acid sites (both the sulfate-free and sulfated SiO_x and PO_x promoted catalysts) is not detrimental to the SCR performance of the 5%WO_3/1%V_2O_5/TiO_2 catalyst system, as the SiO_x promoted catalyst was highly SCR active despite possessing only Brønsted acid sites. The distinction between the two types of acid sites becomes blurrier *in situ* due to the rapid conversion from NH_3 * to NH_4^+* surface species in the presence of moisture [76–78]. The results presented herein further stress that the SCR activity of the 5%WO_3/1% V_2O_5/TiO_2 catalyst system is not dependent on the presence of one acid site type over the other under *ex situ* condition. The most likely source for the promoters' effects on NO conversion is the anchoring of the VO_x active surface sites on the promoted and unpromoted supports. As noted earlier, mainly promoter surface hydroxyls were titrated during the impregnation of 1%V_2O_5 and 5%WO_3. These include both bridging (Al-(OH)-Al and Zr-(OH)-Zr) and terminal (Al-(OH), P-(OH), Si-(OH) and Zr-(OH)) surface hydroxyls generated by the anchoring of the promoters on the TiO_2 support. Such bonds can affect the redox activity of the anchored active sites by a ligand effect, overcoming the promotional effect of the oligomerized surface VO_x as in the case of the PO_x promoted catalyst. The lack of promotional effect from the sulfation of the 5% WO_3/1%V_2O_5/TiO_2 catalyst despite the increase in Brønsted acid sites suggests that there is no connection between the possible promotional effect of the surface SO_x sites and this parameter [13]. The sulfation and impregnation of the non-redox promoters on the surface suppresses the N_2O formation activity of the supported 5%WO_3/1%V_2O_5/TiO_2 catalyst while increasing the Brønsted acid site strength of the catalyst, suggesting an inverse correlation between the Brønsted acid site strength and the N_2O generation propensity of the catalysts (Table 1). This effect on N_2O generation is possibly derived from the role of the acid sites in the ammonia N-H bond breaking rate determining step for the production of N_2O [8], where the stronger acid sites may inhibit the further oxidation of the NH_2- group in the NO-NH_2 surface intermediate that leads to the formation of the N_2O.

4. Conclusions

This work presents for the first time the fundamental Raman- and IR-derived structure-acidity-activity-selectivity relations of sulfated and sulfate-free AlO_x, PO_x, SiO_x and ZrO_x promoted supported V_2O_5-WO_3/TiO_2 SCR catalysts. The promoters were shown to generate unique surface hydroxyl sites that serve to anchor the vanadia and tungsta surface species. The variable acid site character and strength of the promoted catalysts demonstrated the ability to tune the surface acidity of the V_2O_5-WO_3/TiO_2 catalytic system by promoter impregnation and inhibit the formation of the greenhouse gas N_2O by increasing the Brønsted acid site strength. While all promoters suppressed N_2O generation to some extent even when sulfated, the AlO_x and PO_x promoted catalysts exhibited inferior NO conversion activity relative to the unpromoted catalyst both before and after sulfation. Conversely, both the SiO_x and ZrO_x promoted catalysts achieved comparable NO_x activity compared to the unpromoted catalyst when sulfate-free, but lost the promotional effect after sulfation. While the effect of industrial levels of water on the molecular structures and SCR performance of the non-redox promoted catalysts was not investigated in this work, it will be examined in a future study. The effects of the surface promoters on NO conversion are attributed to ligand-effects derived from the anchoring of VO_x and WO_x surface sites on the various promoter metal oxides. Overall, the promoted catalysts investigated herein demonstrate enhanced nitrous oxide suppression capabilities with ranging SCR activity, making them promising candidates for future industrial applications.

CRediT authorship contribution statement

Mingyu Guo: Investigation, Writing – original draft. **Bar Mosevitzky Lis:** Investigation, Writing – original draft, Writing – review & editing, Visualization. **Michael E. Ford:** Supervision. **Israel E. Wachs:** Conceptualization, Supervision, Writing – review & editing, Project administration, Funding acquisition.

Declaration of Competing Interest

The authors declare that they have no known competing financial interests or personal relationships that could have appeared to influence the work reported in this paper.

Acknowledgments

This work was supported as part of Understanding & Control of Acid Gas-Induced Evolution of Materials for Energy (UNCAGE-ME), an Energy Frontier Research Center funded by the U.S. Department of Energy, Office of Science, Basic Energy Sciences under Award # DE-SC0012577. Ms. Mingyu Guo is grateful for the financial support of the scholarship from Tianjin University Graduate School and China Scholarship Council (201906250104).

Appendix A. Supporting information

Supplementary data associated with this article can be found in the online version at doi:10.1016/j.apcatb.2022.121128. References [51-78] are included in the SI" in the "Appendix A Supporting information.

References

[1] R.M. Heck, Catalytic abatement of nitrogen oxides–stationary applications, Catal. Today 53 (1999) 519–523, https://doi.org/10.1016/S0920-5861(99)00139-X.
[2] L. Lietti, I. Nova, G. Ramis, L. Dall'Acqua, G. Busca, E. Giamello, P. Forzatti, F. Bregani, Characterization and reactivity of V_2O_5–MoO_3/TiO_2 de-NOx SCR catalysts, J. Catal. 187 (1999) 419–435, https://doi.org/10.1006/jcat.1999.2603.
[3] Y. He, M.E. Ford, M. Zhu, Q. Liu, Z. Wu, I.E. Wachs, Selective catalytic reduction of NO by NH_3 with WO_3-TiO_2 catalysts: influence of catalyst synthesis method, Appl. Catal. B Environ. 188 (2016) 123–133, https://doi.org/10.1016/j.apcatb.2016.01.072.
[4] H. Chen, Y. Xia, R. Fang, H. Huang, Y. Gan, C. Liang, J. Zhang, W. Zhang, X. Liu, The effects of tungsten and hydrothermal aging in promoting NH_3-SCR activity on V_2O_5/WO_3-TiO_2 catalysts, Appl. Surf. Sci. 459 (2018) 639–646, https://doi.org/10.1016/j.apsusc.2018.08.046.
[5] P.G.W.A. Kompio, A. Brückner, F. Hipler, G. Auer, E. Löffler, W. Grünert, A new view on the relations between tungsten and vanadium in V_2O_5-WO_3/TiO_2 catalysts for the selective reduction of NO with NH3, J. Catal. 286 (2012) 237–247, https://doi.org/10.1016/j.jcat.2011.11.008.
[6] N.R. Jaegers, J. Lai, Y. He, E. Walter, D.A. Dixon, M. Vasiliu, Y. Chen, C. Wang, M. Y. Hu, K.T. Mueller, I.E. Wachs, Y. Wang, J.Z. Hu, Mechanism by which tungsten oxide promotes the activity of supported V_2O_5/TiO_2 catalysts for NOx abatement: structural effects revealed by 51 V MAS NMR spectroscopy, Angew. Chem. Int. Ed. 58 (2019) 12609–12616, https://doi.org/10.1002/anie.201904503.
[7] Y. He, M.E. Ford, M. Zhu, Q. Liu, U. Tumuluri, Z. Wu, I.E. Wachs, Influence of catalyst synthesis method on selective catalytic reduction (SCR) of NO by NH_3 with V_2O_5-WO_3/TiO_2 catalysts, Appl. Catal. B Environ. 193 (2016) 141–150, https://doi.org/10.1016/j.apcatb.2016.04.022.
[8] M. Zhu, J.-K. Lai, I.E. Wachs, Formation of N_2O greenhouse gas during SCR of NO with NH_3 by supported vanadium oxide catalysts, Appl. Catal. B Environ. 224 (2018) 836–840, https://doi.org/10.1016/j.apcatb.2017.11.029.
[9] Y. Peng, W. Si, X. Li, J. Chen, J. Li, J. Crittenden, J. Hao, Investigation of the poisoning mechanism of lead on the CeO_2 - WO_3 catalyst for the NH3-SCR reaction via in situ IR and Raman spectroscopy measurement, Environ. Sci. Technol. 50 (2016) 9576–9582, https://doi.org/10.1021/acs.est.6b02307.
[10] R.M. Heck, R.J. Farrauto, Automobile exhaust catalysts, Appl. Catal. A Gen. 221 (2001) 443–457, https://doi.org/10.1016/S0926-860X(01)00818-3.
[11] J.P. Dunn, P.R. Koppula, H.G. Stenger, I.E. Wachs, Oxidation of sulfur dioxide to sulfur trioxide over supported vanadia catalysts, Appl. Catal. B Environ. 19 (1998) 103–117, https://doi.org/10.1016/S0926-3373(98)00060-5.
[12] L. Han, S. Cai, M. Gao, J. Hasegawa, P. Wang, J. Zhang, L. Shi, D. Zhang, Selective catalytic reduction of NO_x with NH_3 by using novel catalysts: state of the art and future prospects, Chem. Rev. 119 (2019) 10916–10976, https://doi.org/10.1021/acs.chemrev.9b00202.
[13] R. Xie, L. Ma, Z. Li, Z. Qu, N. Yan, J. Li, Review of sulfur promotion effects on metal oxide catalysts for NO x emission control, ACS Catal. 11 (2021) 13119–13139, https://doi.org/10.1021/acscatal.1c02197.
[14] M. Qing, S. Su, L. Wang, L. Liu, K. Xu, L. He, X. Jun, S. Hu, Y. Wang, J. Xiang, Getting insight into the oxidation of SO_2 to SO_3 over V_2O_5-WO_3/TiO_2 catalysts: reaction mechanism and effects of NO and NH3, Chem. Eng. J. 361 (2019) 1215–1224, https://doi.org/10.1016/j.cej.2018.12.165.
[15] H. Kamata, H. Ohara, K. Takahashi, A. Yukimura, Y. Seo, SO_2 oxidation over the V_2O_5/TiO_2 SCR catalyst, Catal. Lett. 73 (2001) 79–83, https://doi.org/10.1023/A:1009065030750.
[16] J.P. Dunn, H.G. Stenger, I.E. Wachs, Oxidation of SO_2 over supported metal oxide catalysts, J. Catal. 181 (1999) 233–243, https://doi.org/10.1006/jcat.1998.2305.
[17] L. Duan, Q. Yu, Q. Zhang, Z. Wang, Y. Pan, T. Larssen, J. Tang, J. Mulder, Acid deposition in Asia: emissions, deposition, and ecosystem effects, Atmos. Environ. 146 (2016) 55–69, https://doi.org/10.1016/j.atmosenv.2016.07.018.
[18] K. Yasuyosh, I. Naomi, K. Keiichiro, Exhaust gas purification catalyst suppressing influence of iron compound, US 9186657 B2, 2015.
[19] T. Masuda, M. Takahito, H. Koji, Flue gas treatment system and flue gas treatment method, US 2016/0129395 A1, 2016.
[20] I. Kiyoshi, I. Yasuyoshi, K. Naomi, Denitration catalyst for ammonia catalytic reduction of nitrogen oxide in flue gas, JP 2013116428, 2013.
[21] S. Hikazudani, N. Hino, Slurry for production of denitration catalyst, process for producing of the slurry, process for producing denitration catalyst by using the slurry, and denitration catalyst produced the process, US 8133833 B2, 2012.
[22] S. Hikazudani, N. Hino, S. Yamamoto, Denitration catalyst and method for producing same, US 2016/0271587 A1, 2016.
[23] S. Li, W. Huang, H. Xu, T. Chen, Y. Ke, Z. Qu, N. Yan, Alkali-induced deactivation mechanism of V_2O_5-WO_3/TiO_2 catalyst during selective catalytic reduction of NO by NH_3 in aluminum hydrate calcining flue gas, Appl. Catal. B Environ. 270 (2020), 118872, https://doi.org/10.1016/j.apcatb.2020.118872.
[24] R. Ning, L. Chen, E. Li, X. Liu, T. Zhu, Applicability of V_2O_5-WO_3/TiO_2 catalysts for the SCR denitrification of alumina calcining flue gas, Catalysts 9 (2019) 220, https://doi.org/10.3390/catal9030220.
[25] T. Yan, Q. Liu, S. Wang, G. Xu, M. Wu, J. Chen, J. Li, Promoter rather than Inhibitor: phosphorus incorporation accelerates the activity of V_2O_5-WO_3/TiO_2 catalyst for selective catalytic reduction of NOx by NH3, ACS Catal. 10 (2020) 2747–2753, https://doi.org/10.1021/acscatal.9b05549.
[26] J. Miao, X. Yi, Q. Su, H. Li, J. Chen, J. Wang, Poisoning effects of phosphorus, potassium and lead on V_2O_5-WO_3/TiO_2 catalysts for selective catalytic reduction with NH3, Catalysts 10 (2020) 345, https://doi.org/10.3390/catal10030345.
[27] K.B. Nam, J.H. Yeo, S.C. Hong, Study of the phosphorus deactivation effect and resistance of vanadium-based catalysts, Ind. Eng. Chem. Res. 58 (2019) 18930–18941, https://doi.org/10.1021/acs.iecr.9b01404.
[28] J. Schobing, V. Tschamber, J.F. Brilhac, A. Auclaire, R. Vonarb, Investigation of the impact of calcium, zinc and phosphorus on denox activity of a commercial SCR catalyst, Top. Catal. 59 (2016) 1013–1019, https://doi.org/10.1007/s11244-016-0583-1.
[29] S. Dahlin, J. Englund, H. Malm, M. Feigel, B. Westerberg, F. Regali, M. Skoglundh, L.J. Pettersson, Effect of biofuel- and lube oil-originated sulfur and phosphorus on the performance of Cu-SSZ-13 and V_2O_5-WO_3/TiO_2 SCR catalysts, Catal. Today 360 (2021) 326–339, https://doi.org/10.1016/j.cattod.2020.02.018.
[30] Z. Yan, W. Shan, X. Shi, G. He, Z. Lian, Y. Yu, Y. Shan, J. Liu, H. He, The way to enhance the thermal stability of V_2O_5-based catalysts for NH_3-SCR, Catal. Today 355 (2020) 408–414, https://doi.org/10.1016/j.cattod.2019.07.037.
[31] X. Liu, H. Chen, X. Wu, L. Cao, P. Jiang, Q. Yu, Y. Ma, Effects of SiO_2 modification on the hydrothermal stability of the V_2O_5/WO_3–TiO_2 NH_3-SCR catalyst: TiO_2 structure and vanadia species, Catal. Sci. Technol. 9 (2019) 3711–3720, https://doi.org/10.1039/C9CY00385A.
[32] X. Liu, X. Wu, T. Xu, D. Weng, Z. Si, R. Ran, Effects of silica additive on the NH_3-SCR activity and thermal stability of a V_2O_5/WO_3-TiO_2 catalyst, Chinese, J. Catal. 37 (2016) 1340–1346, https://doi.org/10.1016/S1872-2067(15)61109-3.
[33] X.-Z. Shao, H.-Y. Wang, M.-L. Yuan, J. Yang, W.-C. Zhan, L. Wang, Y. Guo, G.-Z. Lu, Thermal stability of Si-doped V_2O_5/WO_3–TiO_2 for selective catalytic reduction of NOx by NH3, Rare Met 38 (2019) 292–298, https://doi.org/10.1007/s12598-018-1176-x.
[34] A. Marberger, D. Ferri, D. Rentsch, F. Krumeich, M. Elsener, O. Kröcher, Effect of SiO_2 on co-impregnated V_2O_5/WO_3/TiO_2 catalysts for the selective catalytic reduction of NO with NH3, Catal. Today 320 (2019) 123–132, https://doi.org/10.1016/j.cattod.2017.11.037.
[35] D. Ye, R. Qu, S. Liu, C. Zheng, X. Gao, New insights into the decomposition behavior of NH_4HSO_4 on the SiO_2-decorated SCR catalyst and its enhanced SO_2 -resistant ability, ACS Omega 4 (2019) 4927–4935, https://doi.org/10.1021/acsomega.8b03128.
[36] A. Shi, X. Wang, T. Yu, M. Shen, The effect of zirconia additive on the activity and structure stability of V_2O_5/WO_3-TiO_2 ammonia SCR catalysts, Appl. Catal. B Environ. 106 (2011) 359–369, https://doi.org/10.1016/j.apcatb.2011.05.040.
[37] Y. Zhang, L. Wang, J. Li, H. Zhang, H. Xu, R. Xiao, L. Yang, Promotional roles of ZrO_2 and WO_3 in V_2O_5-WO_3/TiO_2-ZrO_2 catalysts for NOx reduction by NH_3: Catalytic performance, morphology, and reaction mechanism, Chin. J. Catal. 37 (2016) 1918–1930, https://doi.org/10.1016/S1872-2067(16)62510-X.
[38] I.E. Wachs, C.J. Keturakis, Monolayer systems, in: Compr. Inorg. Chem. II, Elsevier, 2013, pp. 131–151, https://doi.org/10.1016/B978-0-08-097774-4.00717-8.
[39] N. Katada, M. Niwa, Y. Murakami, Acidic Property of Silica Monolayers on Metal Oxides Prepared by CVD Method, in: 1994: pp. 333–338. https://doi.org/10.1016/S0167–2991(08)61842-X.
[40] H. Alarcón, G. Boschloo, P. Mendoza, J.L. Solis, A. Hagfeldt, Dye-sensitized solar cells based on nanocrystalline TiO_2 films surface treated with Al3+ ions: Photovoltage and electron transport studies, J. Phys. Chem. B 109 (2005) 18483–18490, https://doi.org/10.1021/jp0513521.
[41] I.E. Wachs, J.-M. Jehng, G. Deo, B.M. Weckhuysen, V.V. Guliants, J.B. Benziger, S. Sundaresan, Fundamental studies of butane oxidation over model-supported vanadium oxide catalysts, J. Catal. 170 (1997) 75–88.
[42] J.-M. Jehng, I.E. Wachs, Surface chemistry of silica-titania-supported chromium oxide catalysts, J. Chem. Soc. Faraday Trans. 91 (1995) 953–961, https://doi.org/10.1039/FT9959100953.
[43] M. Zhu, J.-K. Lai, U. Tumuluri, Z. Wu, I.E. Wachs, Nature of active sites and surface intermediates during SCR of NO with NH_3 by supported V_2O_5–WO_3/TiO_2 catalysts, J. Am. Chem. Soc. 139 (2017) 15624–15627, https://doi.org/10.1021/jacs.7b09646.
[44] M.V. Mathieu, M. Primet, P. Pichat, Infrared study of the surface of titanium dioxides. II. Acidic and basic properties, J. Phys. Chem. 75 (1971) 1221–1226, https://doi.org/10.1021/j100679a008.
[45] K.S. Finnie, D.J. Cassidy, J.R. Bartlett, J.L. Woolfrey, I.R. Spectroscopy, of surface water and hydroxyl species on nanocrystalline TiO_2 films, Langmuir 17 (2001) 816–820, https://doi.org/10.1021/la0009240.

[46] A.A. Tsyganenko, V.N. Filimonov, Infrared spectra of surface hydroxyl groups and crystalline structure of oxides, J. Mol. Struct. 19 (1973) 579–589, https://doi.org/10.1016/0022-2860(73)85136-1.
[47] J.-K. Lai, I.E. Wachs, A Perspective on the Selective Catalytic Reduction (SCR) of NO with NH3 by Supported V2O5–WO3/TiO2 Catalysts, ACS Catal. 8 (2018) 6537–6551, https://doi.org/10.1021/acscatal.8b01357.
[48] C. Deiana, E. Fois, S. Coluccia, G. Martra, Surface structure of TiO_2 P25 nanoparticles: infrared study of hydroxy groups on coordinative defect sites, J. Phys. Chem. C 114 (2010) 21531–21538, https://doi.org/10.1021/jp107671k.
[49] L. Arnarson, H. Falsig, S.B. Rasmussen, J.V. Lauritsen, P.G. Moses, The reaction mechanism for the SCR process on monomer V5+ sites and the effect of modified Brønsted acidity, Phys. Chem. Chem. Phys. 18 (2016) 17071–17080, https://doi.org/10.1039/C6CP02274J.
[50] I. Song, J. Lee, G. Lee, J.W. Han, D.H. Kim, Chemisorption of NH_3 on Monomeric Vanadium Oxide Supported on Anatase TiO_2: A Combined DRIFT and DFT Study, J. Phys. Chem. C. 122 (2018) 16674–16682, https://doi.org/10.1021/acs.jpcc.8b02291.